Chapter 6

SEARCH FOR SUPERSYMMETRY IN EVENTS WITH MISSING TRANSVERSE MOMENTUM AND MULTIPLE B-JETS

Supersymmetry (SUSY) [94, 96–100] is an extension of spacetime symmetry (Section 2.2). Not only does SUSY unify fermions and bosons, it also simultaneously solves a number of problems, including the hierachy problem and the nature of dark matter. It is a leading candidate for beyond-the-Standard-Model physics.

Searching for SUSY is one of the main activities at ATLAS. This chapter discusses a SUSY search that targets gluino pair-production, where the final state includes missing transverse energy and multiple jets, of which at least three must be b-jets. Section 6.1 presents an introduction to the gluino pair-production model. Section 6.2 discusses the data and simulation samples that are used in the analysis. Section 6.3 discusses the physics objects involved. Section 6.4 discusses event selection. Section 6.5 discusses analysis strategies and the results of the search. Section 6.6 discusses the interpretation of the search. Finally, some conclusions are given in Section 6.7.

The data was collected in the period 2015–2016, at 13 TeV centre-of-mass energy and corresponds to an integrated luminosity of 36.1 fb^{-1}.

6.1 Gluino Pair-Production

The hierachy problem in the Standard Model (Section 2.2.1) is solved in SUSY provided the superpartners of the top quarks, the stops, are relatively light (masses at the electroweak scale $\sim$ O(100) GeV) [95]. This in turn implies the superpartners of the gluons, the gluinos, to have masses $\sim$ O(1) TeV. In R-parity conserving SUSY theories, the gluinos are produced in pairs with a cross section much larger than the cross section for direct pair produced stops. As a result, searching for gluinos decaying into stops and sbottoms is highly motivated at ATLAS.

The gluino pair-production models in this analysis are called Gbb and Gtt. They belong to the class of simplified models [101, 102], and are used to optimize search event selections as well as to interpret search results. In terms of signature, simplified models always contain at least four b-jets that originate either from gluino or top quark decays, and two neutralinos.

In Gbb and Gtt, the gluinos, which are superpartners of the Standard Model gluons, are hypothesized to be produced in pairs (Figure 6.1). Each of the gluino $\tilde{g}$ in the pair $\tilde{g}\tilde{g}$ is assumed to decay into a $\tilde{b}\bar{b}$ pair (in Gbb) or a $\tilde{t}\bar{t}$ pair (in Gtt) at 100% branching ratio[1]. In both models the supersymmetric $\tilde{t}$ is assumed to be off-shell; this assumption has been found to have no impact on the search while at the same time simplifying the analysis and the interpretation of the results. Accordingly the parameters of the models consist of only two parameters, the mass of $\tilde{g}$ and the mass of $\tilde{\chi}_1^0$. The $\tilde{\chi}_1^0$'s are assumed to be the lightest supersymmetric particles; they are stable and serve as candidates for dark matter.

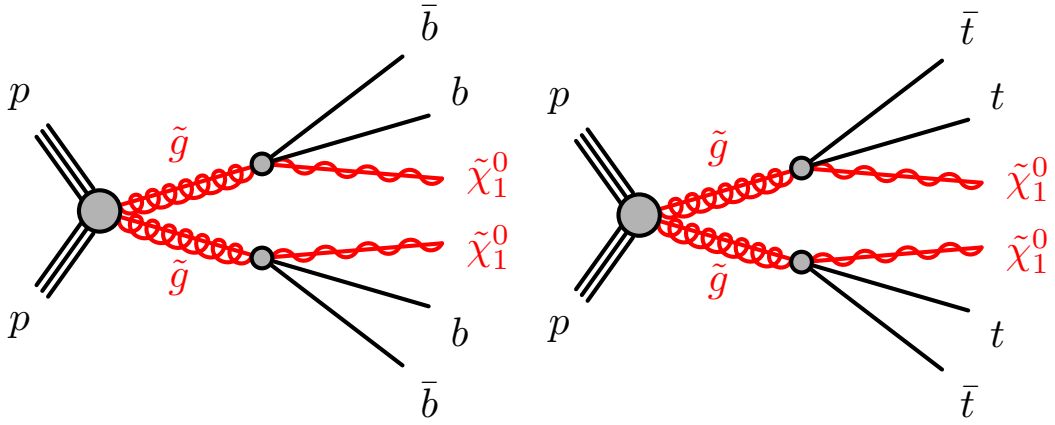

Figure 6.1: The Gbb and Gtt models. Both belong to the class of simplified SUSY models. In both models, the supersymmetric $\tilde{t}$ is assumed to be off-shell. The parameters of the models are the mass of $\tilde{g}$ and the mass of $\tilde{\chi}_1^0$.

In the present chapter the Gtt model search is discussed in detail[2]. Because of the top quark decay mode $t \to Wb$, and the subsequent decays of the four W bosons, we expect signal regions in Gtt to have higher jet multiplicity than those in Gbb. The final state is anticipated to consist of

- Four b-jets from the decays of the four top quarks.
- As many as twelve jets if all W bosons' decays are purely hadronic, or otherwise additional jets and leptons (electrons or muons, the number of which depends on the number of leptonic W boson decays), along with missing transverse energy from the daughter neutrinos of the W bosons and the $\tilde{\chi}_1^0$'s, assuming the latter do not participate in known interactions and manifest themselves as missing transverse energy.

[1] The possibility that one gluino in the pair will decay to $\tilde{t}\bar{b}$ and the other will decay to $\tilde{t}\bar{t}$ is not discussed in the present chapter, however it has been studied [62].

[2] It is connected directly with my contribution to the analysis. This is also, as will be mentioned later, the reason that the chapter focuses on the leptonic final state

The full analysis includes a leptonic and a hadronic channel. In this chapter, only the leptonic final state is discussed in detail; it consists of one or more leptons, large missing transverse energy, and multiple jets in which at least three must be identified as b-jets.

6.2 Data and Simulated Event Samples

The data used in the analysis was collected by the ATLAS detector [52] in the period 2015–2016, delivered by the LHC at 13 TeV centre-of-mas energy and 25 ns bunch spacing. The full data corresponds to an integrated luminosity of 36.1 fb^{-1}, of which the associated uncertainty is 2.1% [53]. An HLT $E_{\mathrm{T}}^{\mathrm{miss}}$ trigger is applied on the data at three online thresholds, 70 GeV for 2015, 100 GeV for early 2016, and 110 GeV for late 2016. The trigger is fully efficient for the events that pass the preselection requirement defined in Section 6.4.2, which imposes the offline condition $E_{\mathrm{T}}^{\mathrm{miss}} > 200$ GeV.

Most signal and background processes are generated using simulations, described below. An exception is the multi-jet process, which is estimated from data. All simulated event samples were passed through the full ATLAS detector simulation using Geant4 [103].

SUSY signal samples The signal processes, where gluino pairs $\tilde{g}\tilde{g}$ are produced and each member in the pair decays according to $\tilde{g} \to t\bar{t}\tilde{\chi}_1^0$, are generated up to two additional partons using MadGraph5_aMC@NLO [54] at leading order, the parton distribution function (PDF) set being NNPDF 2.3 [55]. The samples are interfaced to Pythiav8.186 [56] for parton showering, hadronization, and underlying events. All signal samples are normalized with NLO cross-section calculations.

Standard Model background samples The dominant background is $t\bar{t}$ plus high p_T jets. It is generated with the Powheg-Box [58] v2 event generator using the CT10 [59] PDF set, interfaced with Pythiav6.428. Events in which all the top quarks decay hadronically are excluded because of insufficient $E_{\mathrm{T}}^{\mathrm{miss}}$ to constitute a significant background.

The Powheg-Box v2 event generator is also used for single top quark in the Wt- and s- channels, along with the CT10 PDF set and Pythiav6.428. Powheg-Box v1 is used for the t- channel process. All events with at least one W boson that decays leptonically are included, and events in which all top quarks decay hadronically are excluded because of insufficient $E_{\mathrm{T}}^{\mathrm{miss}}$.

Smaller background contributions include $t\bar{t}$ plus $W/Z/h$ possibly along with jets, and $t\bar{t}t\bar{t}$, W/Z+jets, and $WW/WZ/ZZ$ events. Their generations are described below:

- $t\bar{t}$ plus W/Z: MadGraph5_aMC@NLO v2.2.2 and Pythiav8.186. The PDF set is NNPDF 2.3.
- $t\bar{t}h$: MadGraph5_aMC@NLOv2.2.1 and Herwig++ [60] v2.7.1. The PDF set is CT10.

- $t\bar{t}t\bar{t}$: MadGraph5_aMC@NLOv2.2.2 and Pythiav8.186.
- W/Z+jets: Sherpav2.2.0 [61] and the NNPDF 3.0 PDF set.
- $WW/WZ/ZZ$: Sherpav2.1.1 and the CT10 PDT set.

Other potential sources of backgrounds, such as three top quark or three gauge boson processes, have been determined to be negligible.

6.3 Physics Objects

Physics objects that are used to select events for the analysis are described in this section. The main objects, electrons, muons, and jets, are required to undergo an overlap removal procedure to remove double-counting. The overlap removal procedure is described in the section as well.

Interaction vertices Each interaction vertex in the event is required to be associated with at least two tracks, each of which must have $p_T > 0.4$ GeV. The primary vertex is defined to be the vertex that has the largest sum of squares of transverse momenta of the associated tracks [63].

Jets Candidate jets are reconstructed using the anti-k_t jet algorithm [64, 67, 68] with a radius parameter $\Delta R = 0.4$; these jets will be referred to as small R-jets. They are required to have $p_T > 20$ GeV and $|\eta| < 2.8$, and must undergo an overlap removal procedure with electrons and muons, described below, after which they are required to pass the requirement $p_T > 30$ GeV.

An event is rejected if it contains jets that arise from non-collision sources or detector noise or pile-up interactions [69].

b-jets The hadronization of a b-quark in the event creates a physics object referred to as a b-jet. A b-hadron has a lifetime of about 10^{-12} s and decays after travelling a short distance (mm) from the primary vertex, creating a secondary vertex from which additional tracks originate (Figure 6.2 [104]). The b-jets in the event are identified by a multivariate algorithm, which relies on three pieces of information: The impact parameters of the tracks that belong to the jets, the secondary vertices that are present in the event, and the flight paths of heavy hadrons inside the jets [70, 71]. Identifying b-jets using the algorithm is referred to as b-tagging. In this analysis the b-tagging working point that correponds to a 77% efficiency for b-jets with $p_T > 20$ GeV is chosen, which has a rejection factor of 6 on charm and 134 on light-jets.

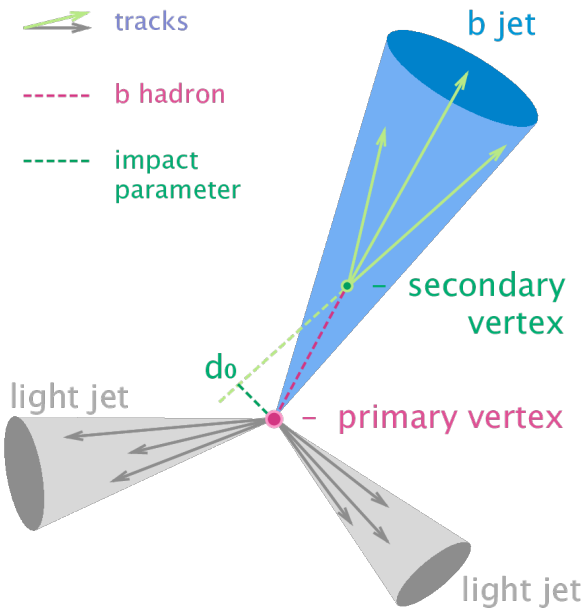

Figure 6.2: b-jet secondary vertex which is displaced with respect to the primary vertex. In addition to tracks that originate from the primary vertex there are tracks that originate from the secondary vertex as well [104].

Large R-jets These jets refer to jets that are built up from the small R-jet candidates [72] that have undergone overlap removals with electrons and muons, using the anti-k_t algorithm with $R = 0.8$. These large R-jets are required to have $p_T > 100$ GeV and $|\eta| < 2.0$. They are a tool to identify boosted top quarks, as a boosted top quark that decays hadronically will produce jets that stay collimated to each other (Figure 6.3). In Gtt, this is expected in events with a large mass difference between the gluino and the neutralino.

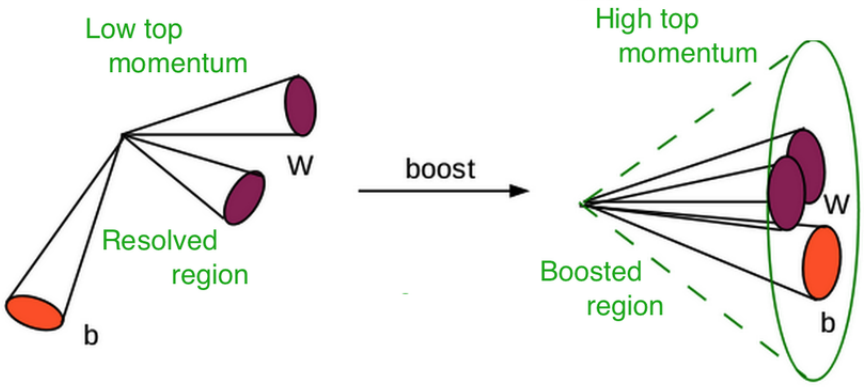

Figure 6.3: Boosted top quark decay (right) compared to low-p_T top quark decay. In the former case, the decay products stay collimated.

Leptons The leptons in the analysis include electrons and muons. Initially, each electron candidate must pass the Loose quality criteria [73, 74] and is required to have $|\eta| < 2.47$. On othe other hand, each muon candidate must pass the Medium

quality criteria [75] and must have $|\eta| < 2.5$.

Subsequently, the leptons undergo overlap removal and those passing this step are required to pass an isolation requirement, in order that fake and non-prompt leptons from jets may be removed. This isolation requirement uses a p_T-dependent cone with radius $\min(0.2, 10\ \text{GeV}/p_T^{\text{lep}})$, where p_T^{lep} is the p_T of the lepton, to take into account the fact that the angular seperation between a lepton in the event and the b-jet narrows as p_T of the top quark increases (Figure 6.3).

Signal leptons are selected as follow. Electrons are required to pass the Tight quality criteria [73, 74]. They are also matched to the primary vertex by requiring the ratio $|d_0|/\sigma_{d_0}$, where d_0 is the transverse impact parameter of the associated ID track and σ_{d_0} is the measured uncertainty of d_0, to be < 5, as well as the longitudinal impact parameter z_0 to satisfy $|z_0 \sin\theta| < 0.5$ mm. On the other hand, muons are matched to the primary vertex by requiring $|d_0|/\sigma_{d_0} < 3$ and $|z_0 \sin\theta| < 0.5$ mm. Events that contain muons with $d_0 > 0.2$ mm or $z_0 > 1$ mm are rejected to suppress cosmic muons.

Missing Transverse Energy This is defined as the magnitude of the negative vector sum of the transverse momenta of all calibrated objects in the event, with an extra term [76, 77] to account for energy deposits not associated with any of the selected objects.

Overlap Removal Electrons, muons, and jets are required to undergo the following sequential overlap removal procedure.

- Electrons found inside $\Delta R < 0.01$ of a muon candidate are removed, to suppress contributions from muon bremsstrahlung.

- Next, overlap removal between electrons and jets are performed, in order to remove electrons reconstructed as jets, which is the case for electrons reconstructed at ATLAS, as well as fake electrons from hadron decays. Thus, non b-jets whose centroids lie within $\Delta R < 0.2$ of electrons are removed, unless the jets are b-jets, because then the electrons are likely to originate from semileptonic b-handron decays. Subsequently, electrons with $E_T < 50$ GeV found within $\Delta R = 0.4$ of jets are removed while the jets are kept. Electrons with higher E_T are likely to be in boosted top quark decays, in which case they are expected to be found closer to the jets the higher are their E_T. Accordingly, a distance that takes into account this fact is used, $\Delta R = \min(0.4, 0.04 + 10\ \text{GeV})/E_T$[3], and any electron found within $\Delta R = 0.4$ of a jet will be treated as a potential signal electron, i.e. an electron will be selected if its E_T justifies its being found close to a jet, but not closer than what its E_T warrants.

- Finally, overlap removal is applied on the remaining muons and jets. If a non b-jet having fewer than three inner detector tracks whose centroid is found

[3]The angular separation ΔR between the decay products of a particle of mass m and tranverse momentum p_T is given approxiamtely by $2m/p_T$.

within a distance $\Delta R = 0.2$ of a muon, the jet is likely to come from high-p_T muon bremsstrahlung and is removed. Then muons with $p_T < 50$ GeV that are found within $\Delta R = 0.4$ of jets are removed, to suppress non-prompt muons originating from jets. Muons having $p_T > 50$ GeV are, as in the case of high E_T electrons, subject to the p_T-dependent overlap removal distance $\Delta R = \min(0.4, 0.04 + 10 \text{ GeV})/p_T$.

Boosted Overlap Removal Studies The use of electrons inside jets had been initiated by the $t\bar{t}$ resonance search [78] in order to gain signal electron acceptance in scenarios that involve the decays of beyond-Standard-Model particles into the Standard-Model top quarks. Following the idea, the p_T-dependent distance $\Delta R = \min(0.4, 0.04 + 10 \text{ GeV})/p_T$ was introduced into the current analysis (first applied to 3.2 fb^{-1} of data) for muons before being subsequently adopted for electrons in a later version of the analysis (at 36.1 fb^{-1}). The study for muons was carried out on three samples, a $t\bar{t}$ sample, a Gtt sample where the mass of the gluino is 1300 GeV and that of the neutralino is 900 GeV, and another Gtt sample where the mass of the gluino is 1600 GeV and that of the neutralino is 100 GeV. The last sample, due to a large mass difference between the gluino and the neutralino, is also called a boosted sample, since it is expected to be a source of boosted top quarks. Figure 6.4, which plots the distance ΔR between the truth level muons and the closest jets, shows a large fraction of potential signal muons below $\Delta R = 0.4$ in the boosted sample. The other signal sample shows a smaller but still considerable fraction of potential signal muons below $\Delta R = 0.4$, most likely due to random overlap between the muons and the top quarks (there are four top quarks as compared to two in the $t\bar{t}$ sample, the latter displays instead a mild peak in the region $\Delta R > 0.4$).

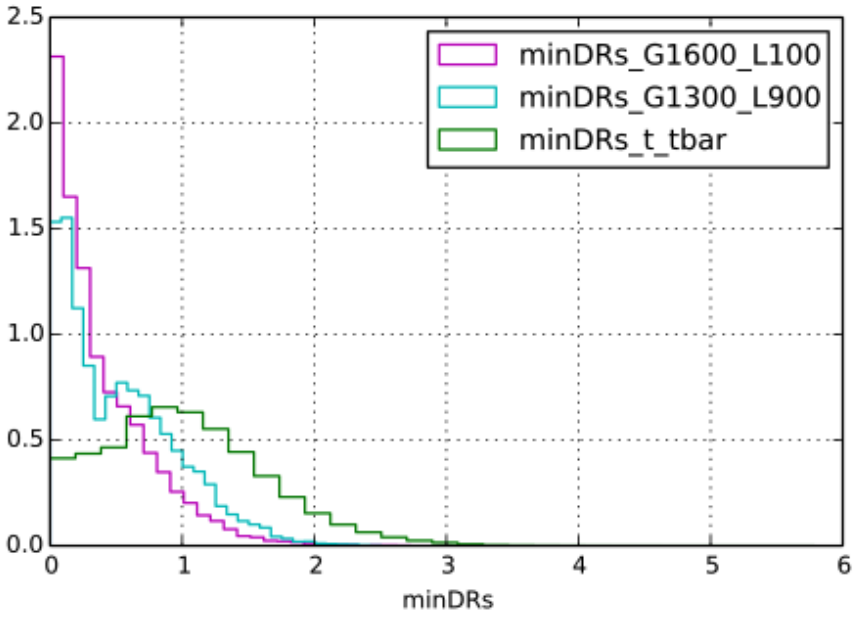

Figure 6.4: ΔR between the truth-level muons and the closest jets. The boosted sample (in pink) where mass of the gluino is 1600 GeV and that of the neutralino is 100 GeV shows a high peak at low ΔR. The other signal sample (in cyan) also displays but not as high. The $t\bar{t}$ sample (in green), exhibits a mild peak around $\Delta R = 1.0$.

In term of the gain in statistical significance, the p_T-dependent overlap removal scheme led to a 15% increase as compared to the scheme in which a fixed $\Delta R = 0.4$ is used.

6.4 Event Selection

In this section the discriminating variables (Section 6.4.1) and the preselection criteria (Section 6.4.2) are discussed. The latter section also includes a discussion of the modelling of the data. Finally, the optimization of some important variables is discussed in Section 6.4.3.

6.4.1 Discriminating Variables

The following list of variables is found to be discriminating between signal and Standard Model backgrounds:

- The effective mass m_{eff}, defined as the sum of missing transverse energy plus the transverse momenta of jets and leptons in the event:

$$m_{\text{eff}} = \sum_i p_T^{\text{jet}_i} + \sum_j p_T^{l_j} + E_{\text{T}}^{\text{miss}}.$$

  This variable is typically much higher for signal events than for background events.

- The transverse mass m_{T}, defined by

$$m_{\mathrm{T}} = \left(2p_T^l E_{\mathrm{T}}^{\mathrm{miss}}(1-\cos(\Delta\phi))\right)^{1/2},$$

where $\Delta\phi$ is the angle between missing transverse momentum of the event and the transverse momentum of the leading lepton.

In background events in which there is one W boson that decays leptonically, such as in semileptonic $t\bar{t}$ and W+jets, this variable reaches a maximum at the value of the W boson mass. It is expected to be higher for signal events where there are additional sources of missing transverse energy such as from the neutralinos.

- The transverse mass $m_{\mathrm{T,min}}^{\text{b-jets}}$ defined by

$$m_{\mathrm{T,min}}^{\text{b-jets}} = \min_{i\leq 3}\left(2p_T^{\text{b-jets}_i} E_{\mathrm{T}}^{\mathrm{miss}}(1-\cos(\Delta\phi))\right)^{1/2},$$

where $\Delta\phi$ is the angle between the missing transverse momentum and the i-th b-jet.

In background $t\bar{t}$ events where a single top quark decays leptonically, this variable reaches a maximum at the value of the top quark mass. It is expected to be higher for signal events because of the additional source of missing transverse energy from the neutralinos.

- The total jet mass M_J^{Σ}, defined by

$$M_J^{\Sigma} = \sum_{i\leq 4} m_{J,i},$$

where $m_{J,i}$ is the mass of the i-th large-radius re-clustered jet in the event. It is higher for signal events, because there are as many as four hadronically decaying top quarks, whereas the background is dominated by $t\bar{t}$ events where one or both of the tops decay leptonically. We note that dilepton $t\bar{t}$ becomes dominant after applying the selections on m_T and $m_{\mathrm{T,min}}^{\text{b-jets}}$ defined above.

6.4.2 Preselection and Modelling of the Data

Preselection The preselection requirements include $E_{\mathrm{T}}^{\mathrm{miss}} > 200$ GeV, in addition to the $E_{\mathrm{T}}^{\mathrm{miss}}$ trigger requirement, at least one electron or muon, and at least four jets of which at least two must be identified as b-jets.

Modelling of the Data In the preselection sample, correction factors need to be extracted to account for shape discrepancies between data and the expected background for m_{eff}. Thus, background-dominated regions are defined by requiring exactly two b-jets and $m_{\mathrm{T,min}}^{\text{b-jets}} < 140$ GeV, in which the correction factors are taken to be the ratio of the number of observed events to the predicted number of background

events in a given m_{eff} bin. The correction factors range from 0.7 to 1.1; they are also taken as an uncertainty for both background and signal events.

Figure 6.5 show a number of variables after preselection, including the number of jets, the number of b-jets, $E_{\text{T}}^{\text{miss}}$, m_{eff}, M_J^{Σ}, and m_{T}, all having had the m_{eff} correction factor applied. The uncertainties shown include the statistical and experimental systematic uncertainties (Section 6.5.3), but exclude the theoretical uncertainties in background modelling.

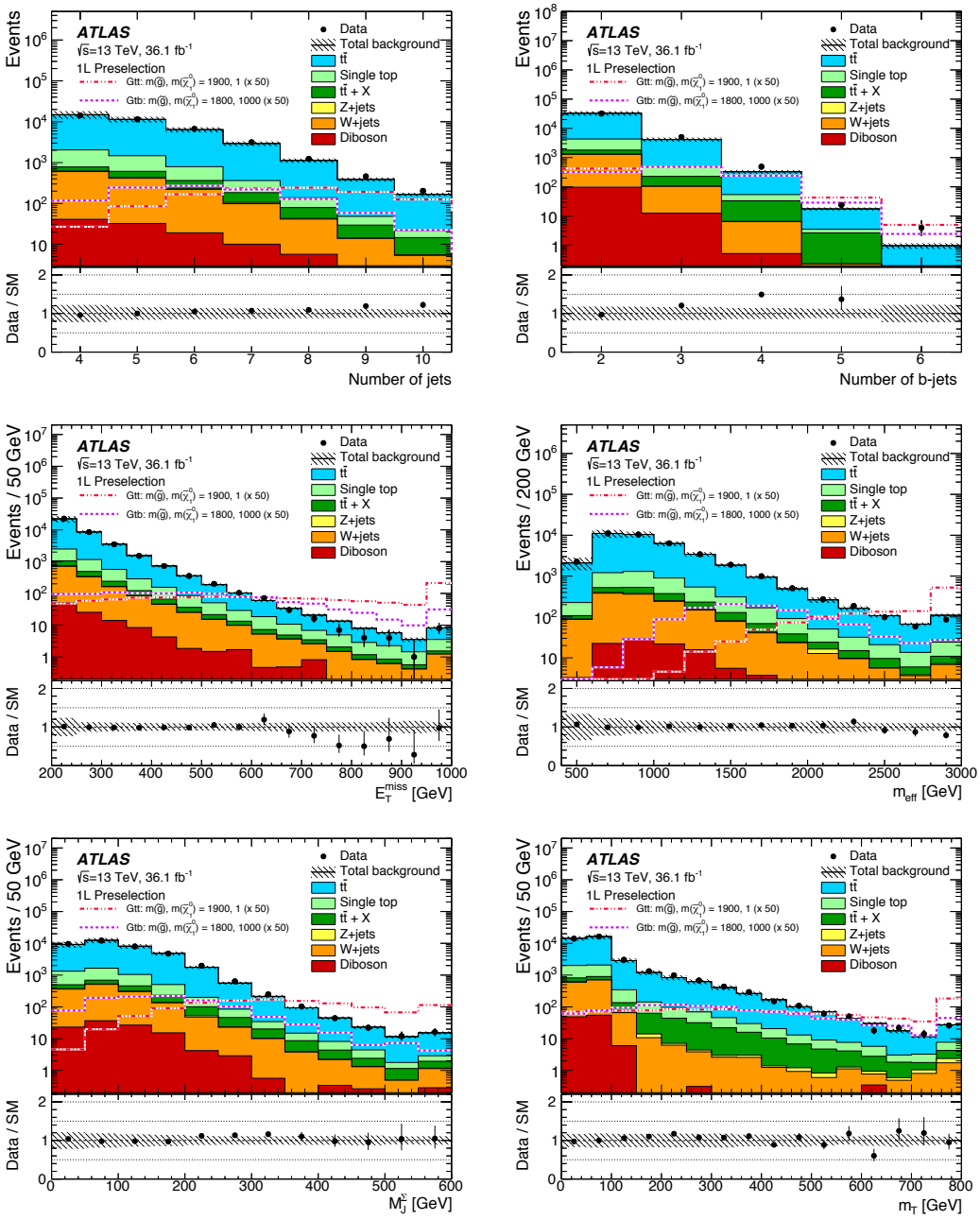

Figure 6.5: The distributions of the number of jets, the number of b-jets, $E_{\mathrm{T}}^{\mathrm{miss}}$, m_{eff}, M_J^{Σ}, and m_{T} after the preselection requirements. The uncertainty includes both statistical and experimental systematatic uncertainties (defined in Section 6.5.3). The last bin includes overflow events. The ratio of data to background prediction is also shown below each figure.

1485

6.4.3 Optimization of Discriminating Variables

An optimization study was performed, at 25 fb^{-1} luminosity, to optimize the selections for the leptonic channel of the analysis[4].

The number of jets (Section 6.3), N_{jet}, missing transverse energy, $E_{\text{T}}^{\text{miss}}$, and m_{eff} are important variables that help with separating signal and background events. In the current analysis, a study was performed to decide on the optimal values of these variables (and of other potentially discriminating variables also). To this end, four samples were selected; they may be put into three groups:

- One sample where the mass of the gluino is 1900 GeV and that of the neutralino is 200 GeV. This will be referred to as the boosted sample, since it is expected to be a source of boosted top quarks.
- One sample where the mass of the gluino is 1900 GeV and that of the neutralino is 1000 GeV; this is a moderately boosted sample.
- Two samples in which the mass differences between the gluino and the neutralino are small. One sample has 1200 GeV and 800 GeV, and one has 1500 GeV and 1000 GeV, which will be called compressed samples number one and two respectively.

The optimization proceeds with different sets of values of potentially discriminating variables, among them including sets in which

- $N_{\text{jet}} \geq 6$, or $N_{\text{jet}} \geq 7$, or $N_{\text{jet}} \geq 8$, or $N_{\text{jet}} \geq 9$, or $N_{\text{jet}} \geq 10$;
- $E_{\text{T}}^{\text{miss}} > 200$ GeV, or $E_{\text{T}}^{\text{miss}} > 300$ GeV, or $E_{\text{T}}^{\text{miss}} > 400$ GeV, or $E_{\text{T}}^{\text{miss}} > 500$ GeV, or $E_{\text{T}}^{\text{miss}} > 600$ GeV;
- m_{eff} is allowed to varied from 500 GeV to 3500 GeV, in steps of 200 GeV.

All possible combinations of the values of the variables are studied. The optimization finds that higher jets improve the search significance, especially for samples in which the mass differences between the gluino and the neutralino are small (the compressed samples). This is consistent with the fact that a small mass difference makes kinematic properties of the signal, such as $E_{\text{T}}^{\text{miss}}$, quite indistinguisable from those of the background, and consequently we have to push to the higher N_{jets} regime. Figure 6.6 shows the significance as the number of jets is allowed to increase while all other variables are kept fixed, for the compressed sample number two. The red point indicates the best significance. Using this result, a higher number of jets was adopted in the definitions of the signal regions discussed in Section 6.5.2.

The optimization also suggests that higher $E_{\text{T}}^{\text{miss}}$ would help when more data becomes available in future LHC run. Figure 6.7 shows the significance as $E_{\text{T}}^{\text{miss}}$ is allowed to increase while all other variables are kept fixed, for the boosted sample where the masses are 1900 GeV and 200 GeV.

[4] As has been mentioned, the chapter focuses only on the leptonic channel and as such the fully hadronic channel, which was optimized separately, is not discussed in the current section.

As for $E_{\mathrm{T}}^{\mathrm{miss}}$, the optimization also suggests higher m_{eff} would help when more data becomes available in future LHC run. Figure 6.8 shows the significance as m_{eff} is allowed to increase while all other variables are kept fixed, for the boosted sample.

The optimization also discovered that the ratio $E_{\mathrm{T}}^{\mathrm{miss}}/m_{\mathrm{eff}}$ was potentially discriminating. This variable has been adopted in the SUSY search with two same-sign leptons [51].

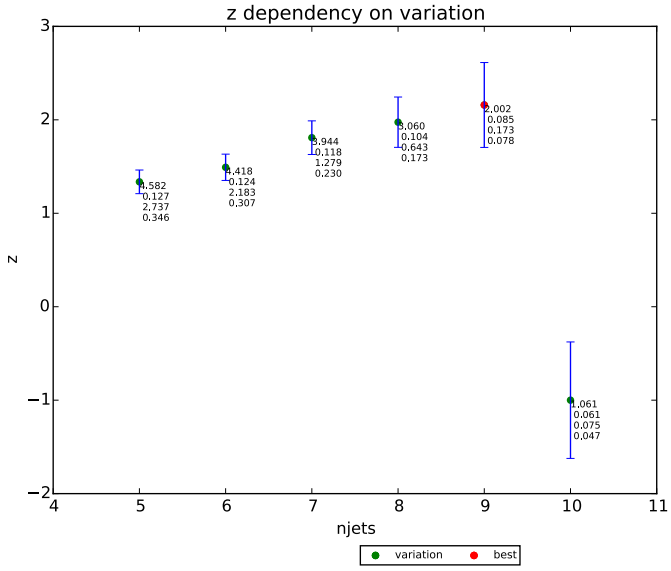

Figure 6.6: The significance with respect to N_{jets} for the compressed sample number two, where the masses are 1500 GeV and 1000 GeV, at 25 fb^{-1} luminosity. The red point indicates the best significance, and the numbers that show up below the points are the signal, the signal uncertainty, the background, and the background uncertainty, in that order. Whenever the calculations of the significance is no longer meaningful, such as when the number of unweighted background events is below 1 event, the significance is set to -1.

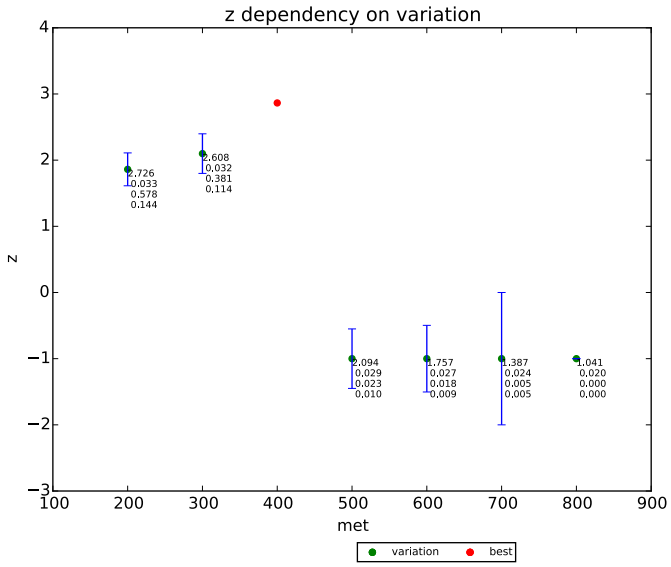

Figure 6.7: The significance with respect to $E_{\mathrm{T}}^{\mathrm{miss}}$ for the boosed sample with masses 1900 GeV and 200 GeV, at 25 fb^{-1} luminosity. The red point indicates the best significance, and the numbers that show up below the points are the signal, the signal uncertainty, the background, and the background uncertainty, in that order.

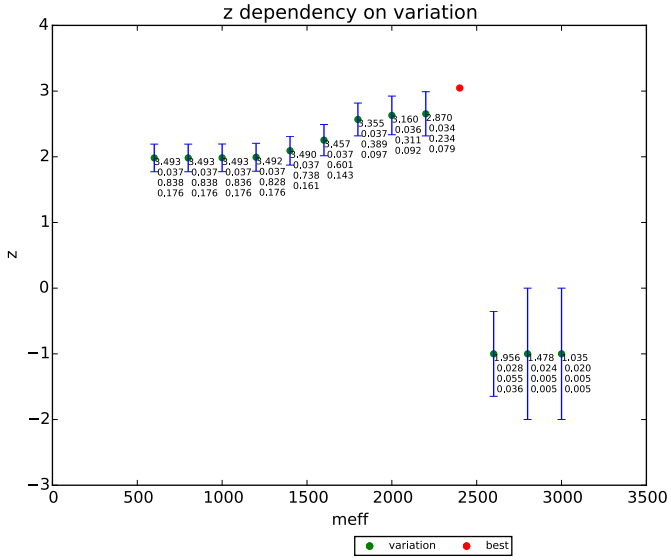

Figure 6.8: The significance with respect to m_{eff} for the boosted sample, where the masses are 1900 GeV and 200 GeV, at 25 fb^{-1} luminosity. The red point indicates the best significance, and the numbers that show up below the points are the signal, the signal uncertainty, the background, and the background uncertainty, in that order.

6.5 Analysis and Results

A significant part of the analysis is the work of background estimation; it is discussed in Section 6.5.1. There are two search strategies, discussed in Section 6.5.2.

Section 6.5.3 discusses the evaluation of systematic uncertainties, and Section 6.5.4 discusses the results of the search.

6.5.1 Background Estimation

Each signal region that is defined is contaminated with Standard Model backgrounds, the dominant source of which is $t\bar{t}$ plus jets, which is estimated using a normalization factor. To this end, in addition to each signal region (SR), a control region (CR), orthogonal to the signal region, but otherwise comparable with it in terms of background composition and kinematics, is defined. Signal contamination in the control region is suppressed by inverting or relaxing some kinematic variables. The normalization factor is then verified in validation regions (VRs), designed to be similar to the signal region in terms of background composition.

The remaining backgrounds are made up of single-top, W+jets, Z+jets, $t\bar{t}$+$W/Z/h$, $t\bar{t}t\bar{t}$ and diboson events. They are estimated from simulations, which are normalized to the best available theoretical cross sections. The multijet background was found to be negligible, but is still estimated using a procedure described in [79].

6.5.2 Analysis Strategy

Physics objects in the final state may fall into different kinematic ranges. These objects consist of those coming from Standard Model events as well as those coming from the hypothetical SUSY events. Naturally, not all kinematic ranges will be equal in terms of the relative distributions of the two kinds of events. The signal and background samples allow us to optimize, i.e. to arrive at one or more sets of kinematic ranges where we will have the best chances to assess whether or not an excess of events, relative to Standard Model distribution, is seen. This assessment can be based solely from judging the excess of events, and is referred to as the cut-and-count strategy. In this strategy, possibly overlapping kinematic regions targetting different gluinos masses are defined, to seek to answer the question if an excess of events is seen at all, in which case we may claim to have seen a signal, or to rule out the existence of any beyond-the-Standard-Model signal, if the number of events seen in fact does not deviate in any statistically significant way from the Standard Model prediction.

On the other hand, if we optimize under the constraint that the signal regions must be non-overlapping with each other, then this constraint could mean that the resulting signal regions might not be as performant as those in the cut-and-count method, in terms of probing the existence of a signal in a single SR. Nevertheless, a combination of these non-overlapping signal regions would take into account many non-overlapping kinematic ranges at the same time, and accordingly would allow us to better assess if the specific model we are using should be ruled out. This strategy is called the multi-bin analysis.

Both strategies are followed in the current analysis for the hadronic channel as well as for the leptonic channel. However, only the leptonic channel will be discussed in the following.

Cut-and-Count Analysis In this analysis strategy the signal points are grouped into three classes. Thus there are three signal regions together with their corresponding control and validation regions. The common selections include ≥ 1 lepton, $p_T^{\text{jet}} > 30$ GeV, and $N_{b\text{-jets}} \geq 3$. The choice of values of other discriminating variables differentiates one class from another. The definitions of the regions are shown in Table 6.1.

- Region B, where B stands for boosted, is optimized for signals having a large mass difference between the gluino and the neutralino (≥ 1.5 TeV).
- Region C, where C stands for compressed, is optimized for signals where the mass difference is small (≤ 300 GeV).
- Region M, where M stands for moderate, is the region where the mass difference is in between those of boosted and compressed regions.

As is shown in the table, the selections on m_{eff}, $E_{\text{T}}^{\text{miss}}$, and M_{J}^{Σ} are lower in signal region C than in signal region B, to improve signal acceptance in the latter. The increase in background as a result of the lower cuts is managed by making tighter selections on the number of jets, the number of b-jets, or $m_{\text{T, min}}^{b\text{-jets}}$. In signal region M, the selections on those variables are intermediate between those of signal region C and signal region C.

The CRs are defined in the low m_{T} region to remove overlaps with the SRs. The $m_{\text{T, min}}^{b\text{-jets}}$ cut is removed, and cuts on other variables are lowered to make sure that each CR would have ≥ 10 events, in order that the normalization of the $t\bar{t}$ background would be determined with sufficient statistical accuracy. On the other hand, there are two types of VRs, VR-m_{T} to validate background prediction in high m_{T} region, and VR-$m_{\text{T, min}}^{b\text{-jets}}$ in the high $m_{\text{T, min}}^{b\text{-jets}}$ region. These VRs are ensured to be kinematically close to the SRs and the CRs by the cut on N_{jets}, which at the same time ensures their non-overlapping. Cuts on other variables are also used to keep the VRs non-overlapping with their corresponding SRs, specifically M_{J}^{Σ} or $m_{\text{T, min}}^{b\text{-jets}}$ in VR-m_{T} and m_T in VR-$m_{\text{T, min}}^{b\text{-jets}}$.

Gtt 1-lepton

Criteria common to all regions: ≥ 1 signal lepton , $p_T^{\text{jet}} > 30$ GeV, $N_{b\text{-jets}} \geq 3$

Targeted kinematics	Type	N_{jet}	m_{T}	$m_{\text{T, min}}^{b\text{-jets}}$	$E_{\text{T}}^{\text{miss}}$	$m_{\text{eff}}^{\text{incl}}$	$M_{\text{J}\Sigma}$
Region B (Boosted, Large Δm)	SR	≥ 5	> 150	> 120	> 500	> 2200	> 200
	CR	$= 5$	< 150	–	> 300	> 1700	> 150
	VR-m_T	≥ 5	> 150	–	> 300	> 1600	< 200
	VR-$m_{\text{T, min}}^{b\text{-jets}}$	> 5	< 150	> 120	> 400	> 1400	> 200
Region M (Moderate Δm)	SR	≥ 6	> 150	> 160	> 450	> 1800	> 200
	CR	$= 6$	< 150	–	> 400	> 1500	> 100
	VR-m_T	≥ 6	> 200	–	> 250	> 1200	< 100
	VR-$m_{\text{T, min}}^{b\text{-jets}}$	> 6	< 150	> 140	> 350	> 1200	> 150
Region C (Compressed, small Δm)	SR	≥ 7	> 150	> 160	> 350	> 1000	–
	CR	$= 7$	< 150	–	> 350	> 1000	–
	VR-m_T	≥ 7	> 150	< 160	> 300	> 1000	–
	VR-$m_{\text{T, min}}^{b\text{-jets}}$	> 7	< 150	> 160	> 300	> 1000	–

Table 6.1: Definitions of the 1-lepton Gtt SRs, CRs and VRs of the cut-and-count analysis. The jet p_T requirement is also applied to b-tagged jets.

Multi-bin Analysis In this analysis strategy a number of non-overlapping regions are defined using N_{jet} and m_{eff}. The regions are shown schematically in Figure 6.9. In each region signal models having a specified range of mass difference are used to optimize all remaining kinematic variables.

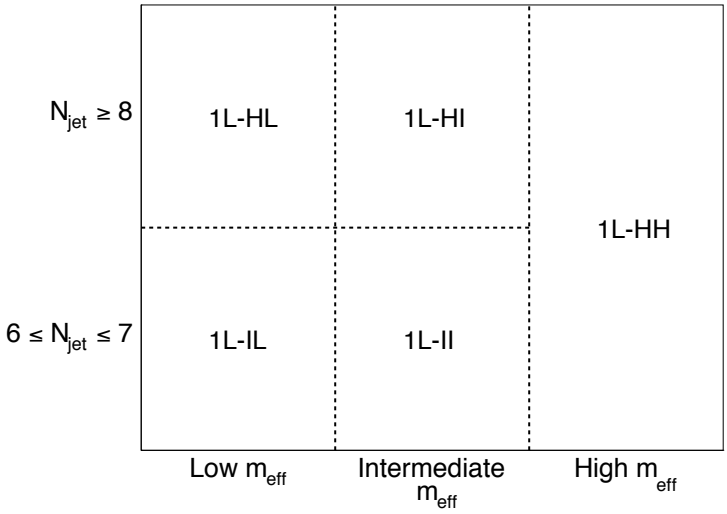

Figure 6.9: Schematic illustration of the regions in the multibin analysis. This is a two-dimensional illustration in the variables N_{jet} and m_{eff}.

The definitions of the regions are shown in Table 6.2, which shows high-N_{jet} SRs, CRs, and VRs, and Table 6.3, which shows intermediate-N_{jet} SRs, CRs, and VRs. The low m_{eff} regions are designed for signals with low mass difference, while the high m_{eff} for boosted events. For each SR, the CR is obtained by keeping most kinematic variables close while inverting the m_{T} cut, so that there would be no overlapping with the SR. The VRs are obtained with cuts on $E_{\text{T}}^{\text{miss}}$ and $m_{\text{T, min}}^{b\text{-jets}}$.

High-N_{jet} regions								
Criteria common to all regions: $N_{b\text{-jets}} \geq 3$, $p_T^{\text{jet}} > 30$ GeV								
Targeted	Type	N_{lepton}	m_{T}	N_{jet}	$m_{\text{T, min}}^{b\text{-jets}}$	M_J^{Σ}	$E_{\text{T}}^{\text{miss}}$	m_{eff}
High-m_{eff} (HH) (Large Δm)	SR-1L	≥ 1	> 150	≥ 6	> 120	> 200	> 500	> 2300
	CR	≥ 1	< 150	≥ 6	> 60	> 150	> 300	> 2100
	VR-1L	≥ 1	> 150	≥ 6	< 140 if $m_{\text{eff}} > 2300$	–	< 500	> 2100
Intermediate-m_{eff} (HI) (Intermediate Δm)	SR-1L	≥ 1	> 150	≥ 8	> 140	> 150	> 300	$[1800, 2300]$
	CR	≥ 1	< 150	≥ 8	> 60	> 150	> 200	$[1700, 2100]$
	VR-1L	≥ 1	> 150	≥ 8	< 140 if $E_{\text{T}}^{\text{miss}} > 300$	–	< 300 if $m_{\text{T, min}}^{b\text{-jets}} > 140$	$[1600, 2100]$
Low-m_{eff} (HL) (Small Δm)	SR-1L	≥ 1	> 150	≥ 8	> 140	–	> 300	$[900, 1800]$
	CR	≥ 1	< 150	≥ 8	> 130	–	> 250	$[900, 1700]$
	VR-1L	≥ 1	> 150	≥ 8	< 140	–	> 225	$[900, 1650]$

Table 6.2: Definition of the high-N_{jet} SRs, CRs and VRs of the multi-bin analysis.

Intermediate-N_{jet} regions								
Criteria common to all regions: $N_{b\text{-jets}} \geq 3$, $p_T^{\text{jet}} > 30$ GeV								
Targeted	Type	N_{lepton}	m_{T}	N_{jet}	$m_{\text{T, min}}^{b\text{-jets}}$	$M_J^{\sum}$	$E_{\text{T}}^{\text{miss}}$	m_{eff}
Intermediate-m_{eff} (II) (Intermediate Δm)	SR-1L	≥ 1	> 150	$[6, 7]$	> 140	> 150	> 300	$[1600, 2300]$
	CR	≥ 1	< 150	$[6, 7]$	> 110	> 150	> 200	$[1600, 2100]$
	VR-1L	≥ 1	> 150	$[6, 7]$	< 140	–	> 225	$[1450, 2000]$
Low-m_{eff} (IL) (Low Δm)	SR-1L	≥ 1	> 150	$[6, 7]$	> 140	–	> 300	$[800, 1600]$
	CR	≥ 1	< 150	$[6, 7]$	> 130	–	> 300	$[800, 1600]$
	VR-1L	≥ 1	> 150	$[6, 7]$	< 140	–	> 300	$[800, 1450]$

Table 6.3: Definition of the intermediate-N_{jet} SRs, CRs and VRs of the multi-bin analysis.

6.5.3 Systematic Uncertainties

The systematic uncertainties on the estimation of the backgrounds come from the extrapolation of the $t\bar{t}$ normalization from the CRs to the SRs, as well as from MC estimations of the minor backgrounds. The total systematic uncertainties vary from 20% to 80%; they are shown in Figure 6.10.

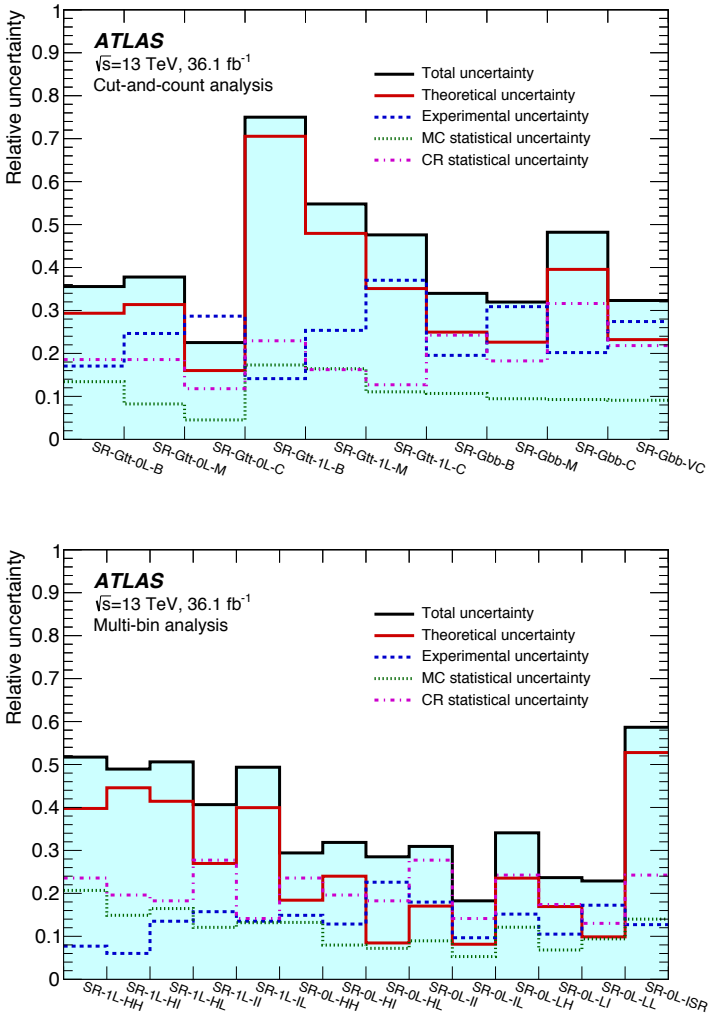

Figure 6.10: Systematic uncertainties for the cut-and-count analysis (top) and multi-bin analysis (bottom).

As $t\bar{t}$ normalization takes place in the CRs, uncertainties due to $t\bar{t}$ simulation only make contributions to the extrapolation from the CRs to the SRs and the VRs.

Among the detector-related uncertainties, the largest contributions come from jet energy scale (JES), jet energy resolution (JER), and the b-tagging efficiencies and mistagging rates. The JES uncertainties are derived from $\sqrt{s} = 13$ TeV data and simulations, whereas the JER uncertainties are derived from 8 TeV data using simulations [80]. These uncertainties are measured for small R-jets and are propagated to re-clustered large R-jets. The jet mass scale and resolution uncertainties make a negligible contribution to re-clustered jet mass. JES uncertainties contribute

between 4% and 35% to the estimation of the backgrounds, and JER uncertainties up to 26%.

The b-tagging and mistagging rate uncertainties contribute between 3% to 24% to the the estimation of the backgrounds. Lepton reconstructions and energy measurement make a negligible contribution.

The theoretical uncertainty on the $t\bar{t}$ background is sum in quadrature of the following sources:

- Hadronization and parton showering model uncertainties are estimated with a POWHEG sample, showered by HERWIG++ v2.7.1 with the UEEE5 underlying-event.

- Uncertainties due to the simulation of initial- and final-state radiation are estimated using POWHEG samples, showered with PYTHIA v6.428. The renormalization and factorization scales are set to twice and then half of their nominal values, so that radiation in the events is increased and decreased respectively. The uncertainty in each case is taken to be the difference between the obtained value and the nominal value.

- The uncertainty due to the choice of matrix-element event generator is estimated by comparing background predictions in MADGRAPH5_aMC@NLO and POWHEG samples, both showered with HERWIG++ v2.7.1.

An additional uncertainty is assigned to $t\bar{t}$ heavy-flavour jets. It was found from simulation studies that each set of SR, CR, and VR had the same fractions of these events. Thus the uncertainties are similar among the regions, and $t\bar{t}$ normalization based on the predictions in the CR largely cancel out these uncertainties. The residual uncertainty is taken as the difference between the $t\bar{t}$ nominal prediction and that obtained after varying the cross-section of $t\bar{t}$ events with additional heavy-flavor jets by 30% [81]. It contributes up to 8% to the total $t\bar{t}$ background uncertainty (background expectation ranges from 5% to 76% in the regions). The statistical uncertainty of the CRs is included in the systematic uncertainties and varies from 10% to 30%.

The single-top simulation suffers from interference between $t\bar{t}$ and Wt processes. This uncertainty is estimated using $WWbb$ events, generated using MADGRAPH5_aMC@NLO, where a comparison is made with the sum of $t\bar{t}$ and Wt processes. Also, uncertainties due to initial- and final-state radiation are estimated using PYTHIA v6.428, as in the case of $t\bar{t}$ uncertainties. Moreover, an additional 5% uncertainty is included in the cross-section of single-top processes [81]. The total uncertainty for the single-top process contributes to a change of the overall background of up to 11% in the regions.

Uncertainties in the W/Z+jets backgrounds are estimated by varying various parameter scales, and make a contribution up to 50% in the regions.

Finally, the uncertainties in the cross-sections of signal processes are determined from an envelope of different cross-section predictions. A systematic uncertainty is also assigned to the kinematic correction described in Section 6.4.2; the total size of the correction is used as an uncertainty.

6.5.4 Results

In each SR, the expected SM background is determined with a profile likelihood fit [82] implemented in the HistFitter framework [83], which will be referred to as a background-only fit. The fit uses as inputs the number of events predicted by simulation in each region, plus the number of events predicted in the associated CR. It is constrained by the number of observed events in the CR and outputs a $t\bar{t}$ normalization factor that is applied to the number of $t\bar{t}$ events predicted by simulation in the SR. The number of observed and predicted events are modelled as Poisson distributions, and the systematic uncertainties as Gaussian distributions having widths that correspond to the sizes of the uncertainties, treated as correlated where appropriate. The likelihood function is the product of the various distributions.

Figure 6.11 shows the values of the normalization factors resulting from the fit, the expected numbers of background events and observed data in all the CRs for the cut-and-count and multi-bin analyses. They can be seen to be mostly consistent with one within uncertainties. The normalization factors for the hadronic Gtt channel and Gbb, not discussed in detail in this chapter, are also shown.

Figure 6.12 shows the results of the fit to the CRs, extrapolated to the VRs for the cut-and-count and multi-bin analyses. The background predicted by the fit is compared to the data in the upper panel. The figure also shows in the lower panel the pull, which is the difference between the observed number of events and the predicted background divided by the total uncertainty. None of the pulls exceeds 2σ and thus no significant mis-modelling is indicated.

Since the agreements in the VRs are satisfactory, the SRs have been unblinded. Figure 6.13 shows the SRs for the cut-and-count and multi-bin analyses. The pull is shown in the lower panel. No significant excess relative to the predicted background is seen. The largest excess is observed in `SR-OL-HH` that belongs to the multi-bin anlaysis, showing a 2.3σ excess [5]. The background is dominated by $t\bar{t}$ in all SRs.

Table 6.4 shows the observed number of events and predicted number of background events from the background fit for the cut-and-count analysis. In general, the central value of the fitted background is larger than the MC-only prediction. This is in part due to an underestimation of the cross-section of $t\bar{t}+ \geq 1b$ and $t\bar{t}+ \geq 1c$ processes in the simulation.

[5] This excess was followed up in a subsequent analysis at 80 fb^{-1} but no longer appeared.

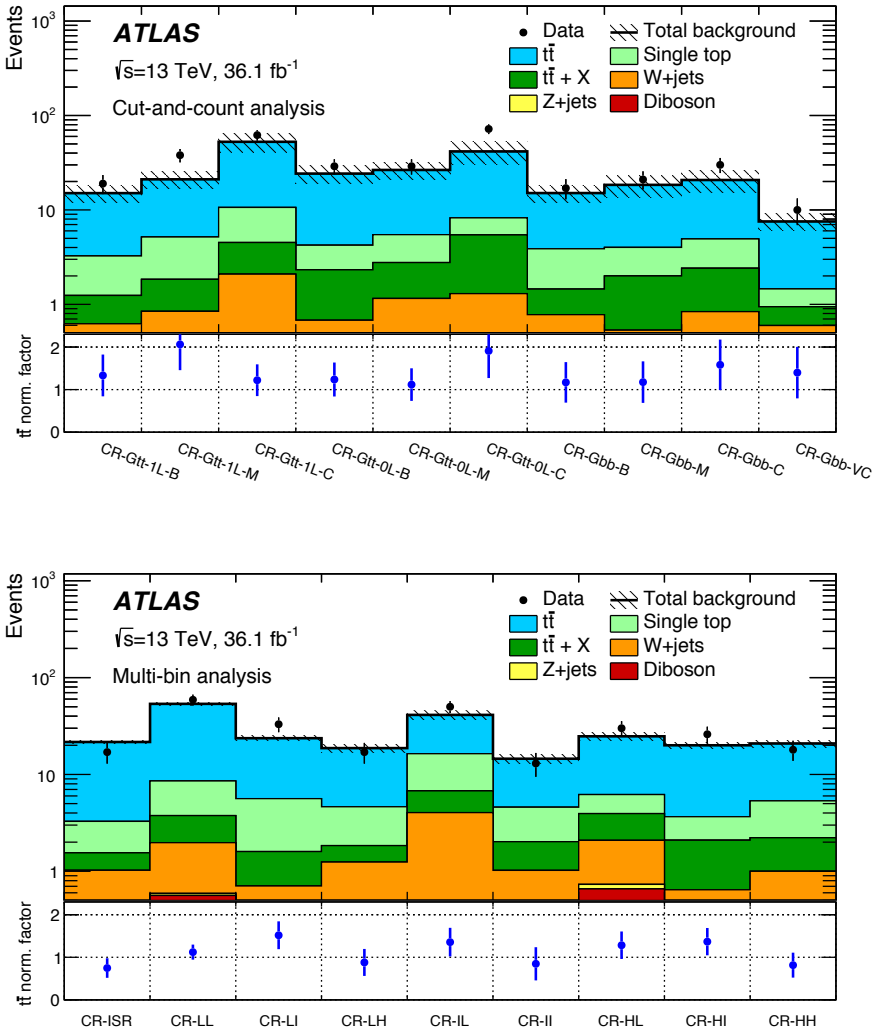

Figure 6.11: Pre-fit events in CRs and the related $t\bar{t}$ normalization factors for the cut-and-count analysis (top) and multi-bin analysis (bottom). The upper panel shows the observed number of events and the predicted background before the fit. The background $t\bar{t}+X$ include $t\bar{t}W/Z$, $t\bar{t}H$, and $t\bar{t}t\bar{t}$ events. The multijet background is negligible. All uncertainties described in Section 6.5.3 are included in the uncertainty band. The $t\bar{t}$ normalization is obtained from the fit and is shown in the bottom panel.

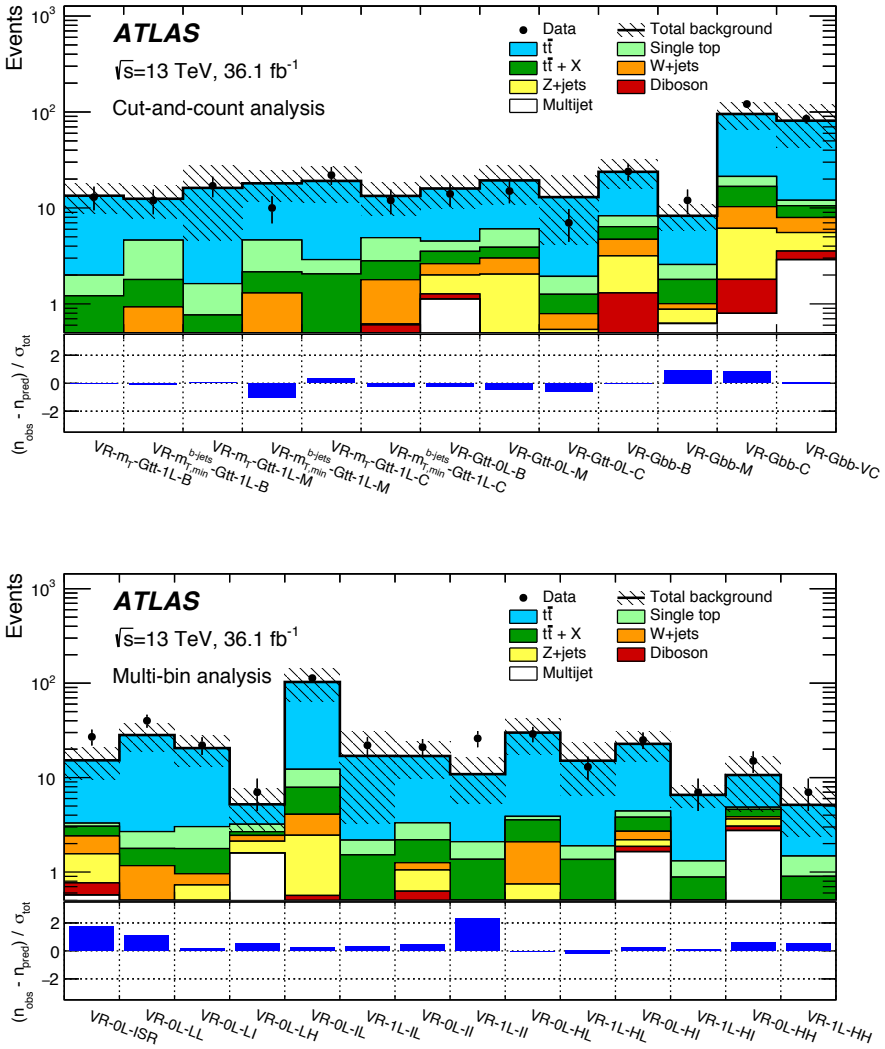

Figure 6.12: Background fit extrapolated to the VRs of the cut-and-count analysis (top) and the multi-bin analysis (bottom). The $t\bar{t}$ normalization is obtained from the fit to the CRs shown in Figure 6.11. The upper panel shows the observed number of events and the predicted background. The background $t\bar{t}+X$ include $t\bar{t}W/Z$, $t\bar{t}H$, and $t\bar{t}t\bar{t}$ events. The lower panel shows the pulls in each VR. The last row displays the total background prediction when the $t\bar{t}$ normalization is obtained from a theoretical calculation [65].

	SR-Gtt-1L		
Targeted kinematics	B	M	C
Observed events	0	1	2
Fitted background	0.5 ± 0.4	0.7 ± 0.4	2.1 ± 1.0
$t\bar{t}$	0.4 ± 0.4	0.5 ± 0.4	1.2 ± 0.8
Single-top	0.04 ± 0.05	0.03 ± 0.06	0.35 ± 0.28
$t\bar{t}+X$	0.08 ± 0.05	0.09 ± 0.06	0.50 ± 0.28
Z+jets	0.049 ± 0.023	0.050 ± 0.023	< 0.01
W+jets	< 0.01	< 0.01	0.024 ± 0.026
Diboson	< 0.01	< 0.01	< 0.01
MC-only background	0.43	0.45	1.9

Table 6.4: Results of the background-only fit extrapolated to the Gtt 1-lepton SRs in the cut-and-count analysis, for the total background prediction and breakdown of the main background sources. The uncertainties shown include all systematic uncertainties. The data in the SRs are not included in the fit. The background $t\bar{t}+X$ includes $t\bar{t}W/Z$, $t\bar{t}H$, and $t\bar{t}t\bar{t}$ events. The row MC-only background provides the total background prediction when the $t\bar{t}$ normalization is obtained from a theoretical calculation [65].

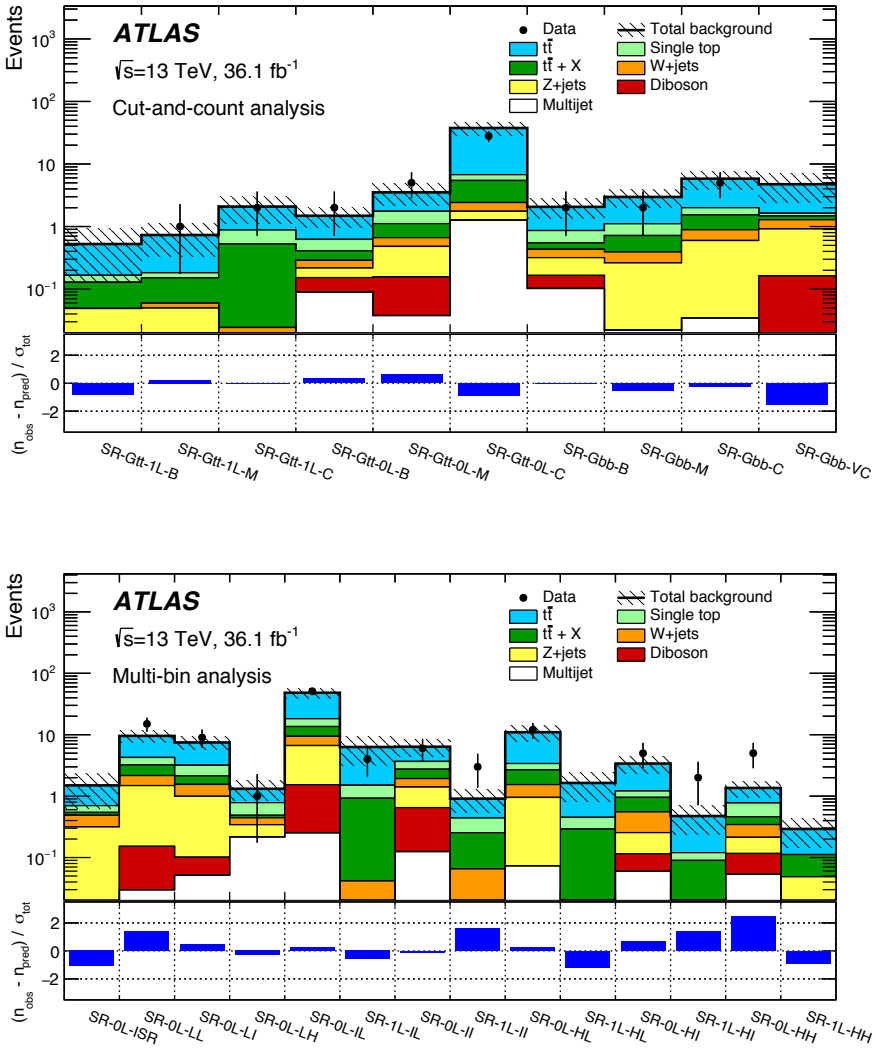

Figure 6.13: Background-only fits extrapolated to the SRs for the cut-and-count analysis (top) and multi-bin analysis (bottom). The data in the SRs are not included in the fit. In each figure the upper panel shows the observed number of events and the predicted background yield. All uncertainties discussed in Section 6.5.3 are included. The background $t\bar{t}+X$ includes $t\bar{t}W/Z$, $t\bar{t}H$, and $t\bar{t}t\bar{t}$ events.The lower panel shows the pulls in each SR.

6.6 Interpretation

No discovery can be claimed and one-sided upper limits at 95% confidence level (CL) are derived from the data. Section 6.6.1 discusses model-independent exclusion limits and Section 6.6.1 discusses model-dependent exclusion limits.

6.6.1 Model-independent Exclusion Limits

For each SR, model-independent limits on the number of beyond-the-SM events are derived. Pseudoexperiments in the CL_s prescription [84] are employed, neglecting possible signal contamination in the CR. Only the single-bin regions in the cut-and-count are used. Table 6.5 shows the results. It includes the visible beyond the Standard Model cross-section (σ^{95}_{vis}) obtained by dividing the observed upper limits on the number of beyond the Standard Model events with the integrated luminosity, as well as the p_0-values, which represent the probability that the SM background alone would fluctuate to the observed number of events or higher.

Signal channel	p_0 (Z)	σ^{95}_{vis} [fb]	S^{95}_{obs}	S^{95}_{exp}
SR-Gtt-1L-B	0.50 (0.00)	0.08	3.0	$3.0^{+1.0}_{-0.0}$
SR-Gtt-1L-M	0.34 (0.42)	0.11	3.9	$3.6^{+1.1}_{-0.4}$
SR-Gtt-1L-C	0.50 (0.00)	0.13	4.8	$4.7^{+1.8}_{-0.9}$

Table 6.5: The p_0-values and Z (the number of equivalent Gaussian standard deviations), the 95% CL upper limits on the visible cross-section (σ^{95}_{vis}), and the observed and expected 95% CL upper limits on the number of BSM events (S^{95}_{obs} and S^{95}_{exp}). The maximum allowed p_0-value is truncated at 0.5.

6.6.2 Model-dependent Exclusion Limits

Multi-bin analysis regions from the leptonic and hadronic channels are statistically combined, using the CL_s prescription in the asymptotic approximation [82], to set model-dependent upper limits, The expected and observed limits are found to be compatible with the CL_s calculated from pseudoexperiments.

Figure 6.14 shows the 95% CL observed and expected exclusion limits in the neutralino and the gluino mass plane. The $\pm 1\sigma^{\text{SUSY}}_{\text{theory}}$ limit lines are obtained by changing the SUSY cross-section by one standard deviation up and down (Section 6.2). The yellow band around the expected limit shows the $\pm 1\sigma$ uncertainty, including all statistical and systematatic uncertainties, except the theoretical uncertainties in the SUSY cross-section. The current search shows an improvement, compared to the previous result performed at $\sqrt{s} = 13$ TeV and 3.2 fb^{-1} integrated luminosity [66], of 450 GeV in gluino mass sensitivity, assuming massless neutralino. Gluinos having masses below 1.97 TeV are excluded at 95% CL for neutralino masses lower than 300 GeV. The red line shows the observed limit; at high gluino mass it is weaker than the expected limits, due to a mild excess observed in the region SR-1L-HI (and a mild excess in a region in the hadronic channel) of the multi-bin analysis.

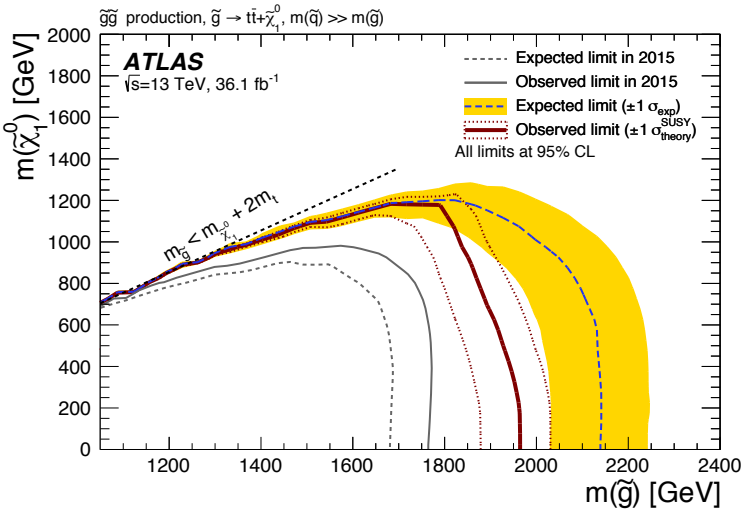

Figure 6.14: Exclusion limits in the multi-bin analysis. The dashed line shows the 95% CL expected limit, and the solid bold line the 95% CL observed limit. The shaded bands around the expected limits show the impact of experimental and background uncertainties. The dotted lines show the impact on the observed limit of the variation of the nominal signal cross-section by $\pm 1\sigma$ of its theoretical uncertainty. Also shown are the 95% CL expected and observed limits from the ATLAS search based on 2015 data [66].

6.7 Conclusions

The analysis in this chapter presents a search for pair-produced gluinos, which is highly motivated at ATLAS as gluinos are expected to have a mass around the TeV scale by naturalness, as well as a high production cross section at the LHC. The data used was collected at the LHC in the 2015-2016 data taking period, at $\sqrt{s} = 13$ TeV and correponded to an integrated luminosity of 36.1 fb^{-1}. The signal model is Gtt, of which the leptonic final state involves at least one lepton, large E_T^{miss}, and multiple jets among which at least three must be b-jets. Several signal regions are defined to accommodate several ranges of mass differences between the gluino and the neutralino. Two analysis strategies are followed, the cut-and-count strategy in which possibly overlapping signal regions are optimized for discovery, and the multi-bin strategy in which non-overlapping signal regions are optimized for model-dependent exclusions. The dominant source of background is $t\bar{t}$+jets, whose normalization factors are obtained in dedicated control regions. No excess relative to the Standard Model background can be claimed. Model-independent limits are set on the visible cross-section for new physics processes. The multibin regions in the leptonic channel are combined with those in the hadronic channel to set model-dependent limits on gluino and neutralino masses. For neutralino masses below approximately 300 GeV, gluino masses of less than 1.97 TeV are excluded at the 95% CL, which is an improvement compared to the exclusion limits obtained with the 2015 dataset alone.